

pubs.acs.org/molecularpharmaceutics Article

Investigating the Mechanisms of Antibody Binding to Alpha-Synuclein for the Treatment of Parkinson's Disease

Malcolm C. Harrison and Pin-Kuang Lai*



Cite This: Mol. Pharmaceutics 2024, 21, 5326-5334



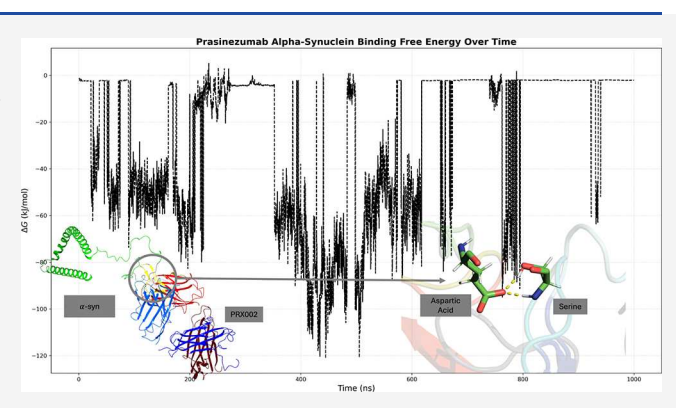
ACCESS I

III Metrics & More

Article Recommendations

Supporting Information

ABSTRACT: Parkinson's disease (PD) is an idiopathic neuro-degenerative disorder with the second-highest prevalence rate behind Alzheimer's disease. The pathophysiological hallmarks of PD are both degeneration of dopaminergic neurons in the substantia nigra pars compacta and the inclusion of misfolded α -synuclein (α -syn) aggregates known as Lewy bodies. Despite decades of research for potential PD treatments, none have been developed, and developing new therapeutic agents is a time-consuming and expensive process. Computational methods can be used to investigate the properties of drug candidates currently undergoing clinical trials to determine their theoretical efficiency at targeting α -syn. Monoclonal antibodies (mAbs) are biological drugs with high specificity, and Prasinezumab (PRX002) is an



mAb currently in Phase II, which targets the C-terminus (AA 118–126) of α -syn. We utilized BioLuminate and PyMol for the structure prediction and preparation of the fragment antigen-binding (Fab) region of PRX002 and 34 different conformations of α -syn. Protein—protein docking simulations were performed using PIPER, and 3 of the docking poses were selected based on the best fit. Molecular dynamics simulations were conducted on the docked protein structures in triplicate for 1000 ns, and hydrogen bonds and electrostatic and hydrophobic interactions were analyzed using MDAnalysis to determine which residues were interacting and how often. Hydrogen bonds were shown to form frequently between the HCDR2 region of PRX002 and α -syn. Free energy was calculated to determine the binding affinity. The predicted binding affinity shows a strong antibody—antigen attraction between PRX002 and α -syn. RMSD was calculated to determine the conformational change of these regions throughout the simulation. The mAb's developability was determined using computational screening methods. Our results demonstrate the efficiency and developability of this therapeutic agent.

KEYWORDS: Parkinson's disease, monoclonal antibodies, protein-protein docking, hydrogen bonds, root mean squared deviation, developability

1. INTRODUCTION

Parkinson's disease (PD) is an idiopathic neurodegenerative disease that affects 2-3% of the population over 65. The pathophysiological hallmarks of PD are the degeneration of dopaminergic neurons in the substantia nigra pars compacta (SNpc), as well as the inclusion of cytotoxic Lewy bodies.² The primary constituent of Lewy bodies is misfolded aggregates of alpha-synuclein $(\alpha$ -syn),³ consisting of 140 amino acid residues encoded by the synuclein alpha (SNCA) gene, which upon mutation, causes familial PD.4 The loss of dopaminergic neurons in the SNpc causes a decrease in dopamine (DA) levels in the corpus striatum, generating deregulation of the basal ganglia systems, leading to motor symptoms such as resting tremor, rigidity, bradykinesia, and loss of static stability.⁵ Depletion of DA levels can reach 80% before any changes in tonic DA can be measured, showing the need to identify PD before the disease has caused irreparable damage. Siderowf et al. showed that α -syn seed amplification assays can

be applied for the accurate identification of PD patients and those at high risk for PD.⁷

The discovery, development, and manufacturing of new drug candidates is a long, laborious, and expensive process, with the average cost for research and development of a single drug candidate at \$1.1 billion.⁸ In the last 30 years, monoclonal antibodies (mAbs) have come into the biopharmaceutical landscape as therapeutic agents rather than tools for scientific analysis.⁹ These medications are highly specific, as they are designed for a specific epitope and have several different routes for administration.¹⁰ MAbs have been developed to treat

Received: August 5, 2024 Revised: August 29, 2024 Accepted: August 30, 2024 Published: September 9, 2024





oncological, cardiovascular, kidney, and neurological diseases. The biggest challenge with developing mAbs for central nervous system disorders is the large size of biological drugs attempting to pass through the blood-brain barrier (BBB). Recent successes in the development of mAbs for Alzheimer's disease (AD) show the promise of targeting and lowering the number of protein aggregates in the brain. Alsheimer is disease to the development of targeting and lowering the number of protein aggregates in the brain.

Prasinezumab (PRX002) is a mAb developed by Roche and Prothena that targets the C-terminus (AA 118-126) of α syn. 16,17 PRX002 is currently in clinical trial stage 2b after a promising phase Ib trial, which showed its high affinity for peripheral α -syn as well as no fatalities, severe adverse effects, or anti-PRX002 antibodies formed. However, the drug was further studied during a phase II trial, and no meaningful effect was observed from PRX002 administration when compared to placebo. 18 The therapeutic is currently undergoing a phase IIb trial titled PADOVA for further analysis of PRX002's ability to slow the progression of motor dysfunction in early-stage PD patients. Another anti- α -syn mAb, Cinpanemab, has also undergone clinical trials but targets a different region of the α syn, the N-terminus. When compared to PRX002, Cinpanemab only binds to aggregated α -syn and does not recognize monomeric or oligomeric forms.²⁰ The Cinpanemab phase II trial ended after there was no meaningful benefit compared to the placebo, so PRX002 is currently the only mAb still in clinical trials for PD.

In the past three decades, computer-aided drug discovery methods have been extremely influential in the biopharmaceutical industry.²¹ The ability to speed up and reduce the price of developing therapeutics is an extremely attractive characteristic of utilizing computational tools in research and development settings. Of these technologies, molecular dynamics (MD) and machine learning (ML) have had the highest influence. MD can be used to simulate interactions between proteins and ligands,²² antibody-antigen binding,²³ as well as discovering novel binding sites.²⁴ ML has great applications for utilizing the physicochemical properties of drug-like compounds to predict if a projected drug will be a successful candidate in both clinical trials and mass production.^{25,26} These tools have been extremely valuable in the search for a cure for challenging diseases, including neurological conditions such as PD²⁷⁻²⁹ and AD.³⁰

The administration of mAbs presents a challenge for PD patients, as the cognitive and motor symptoms of the disease greatly affect driving ability and safety, ³¹ leading to increased dependency on a caregiver for transportation. Subcutaneous (SC) administration of PRX002 would allow PD patients to safely administer this medication from their homes, potentially increasing safety and adherence. The challenge with SC administration is the high concentration of mAbs, which can lead to aggregation and elevated viscosity. ³²

In this paper, we utilize computational methods to model the interactions between the fragment antigen binding (Fab) region of PRX002 with α -syn in silico, simulate binding between these two proteins, perform MD simulations to analyze intermolecular forces taking place at the binding site, calculate the binding free energy of the antibody and antigen, determine the conformational changes of the complementarity determining regions (CDR) of the variable region (Fv) on both the heavy and light chains (V_H and V_L, respectively), as well as test the potential for developability and similarity to clinical-stage therapeutics. This mechanistic study will help evaluate the effectiveness of PRX002 and provide a workflow

to optimize future drug discovery and development, reducing experimental costs and leading to more effective and tailored therapies.

2. MATERIALS AND METHODS

2.1. Generation of Docked PRX002- α -syn Complex. The sequence data for PRX002 was obtained from the Kyoto Encyclopedia of Genes and Genomes (KEGG),³³ and Schrödinger software BioLuminate^{34–38} and PyMol³⁹ were used to predict the protein structure of the Fab region of the mAb, with Chothia numbering used to annotate the final models. An ensemble of thirty-four different confirmations of α -syn was obtained from the Protein Data Bank (PDB ID 2KKW),⁴⁰ gathered by nuclear magnetic resonance (NMR) and electron paramagnetic resonance (EPR) spectroscopy. This ensemble was chosen to have a different conformation of the intrinsically disordered region of α -syn in protein docking. Both proteins were prepared by removing water and adding missing side chain atoms using the Protein Preparation Wizard, 41 and structure reliability reports were completed using BioLuminate. PIPER^{42,43} was used to perform proteinprotein docking on PRX002 and all 34 variations of α -syn. The conformations of 2KKW were rotated to form several different static orientations with respect to PRX002, and each orientation was translated to find the best docking score. The top 1000 rotations are clustered using the RMSD distance between matching atoms. The final structures were those from each cluster with the most neighbors. Refinement was performed on the side chains postprotein docking to reduce

steric clashes and optimize interactions. **2.2. Simulation Preparation.** Using Visual Molecular Dynamics (VMD, version 1.9.3),44 the heavy chain and light chains of PRX002 and α -syn were separated, renumbered, and patches were used between cysteine residues on the Fab region to define the disulfide bridges. The VMD plugin psfgen was then used to create a simulation-ready protein atom coordinate file (pdb) and protein structure file (psf). This structure then underwent minimization for 5000 steps using Nanoscale Molecular Dynamics (NAMD, version 2.14).⁴⁵ Solvation and ionization were performed utilizing the solvate and autoionized VMD plugins using a PDB file generated by the minimization step, with one sodium atom added to neutralize the system, embedding the structure in a solvate box extending 10 Å from the protein boundary (Figure 1). The CHARMM36m force field was utilized in the simulation along the three-point water model (TIP3P) and CHARMM parametrization for water and ions formatted for NAMD.46,47

2.3. Molecular Dynamics. All simulations were performed using VMD and NAMD (versions 2.14 and 3.0alpha). Simulations were run using an A100 GPU on the Anvil highperformance computing cluster. Results from the ionization steps were minimized, heat prepared, and brought to equilibrium before production runs were performed. Simulations were performed at 300 K, kept constant by Langevin dynamics, and pressure at 1.01325 bar, kept constant by a Langevin piston. After energy minimization was performed, the system was heated from 100 to 300 K over 5 K intervals for 200 ps. The integration time step of the simulation was 2 fs per step, with the position coordinates saved every 200 ps in a DCD file. Particle Mesh Ewald (PME)⁴⁸ was used for longrange electrostatic interactions, and a smooth cutoff was implemented for van der Waals forces (10-12 Å). Each system was simulated in triplicate for 1 μ s.

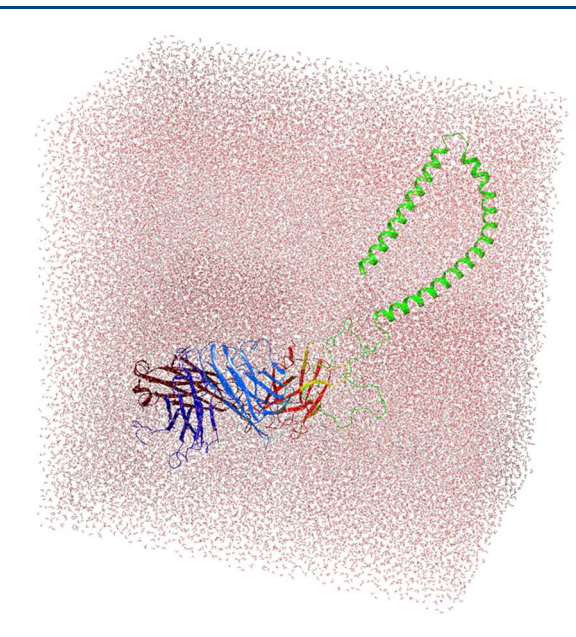


Figure 1. PRX002 and α -syn in a solvated and ionized system. The water and ion boxes extend 10 Å past the edge of the protein boundary. PRX002 = multicolor cartoon, α -syn = green cartoon.

2.4. MDAnalysis. Topology and coordinate files from the MD simulations were exported for descriptive data analysis of hydrogen bonds formed during the simulation. MDAnalysis^{49,50} was used to convert the coordinate files into NumPy⁵¹ arrays and calculate the atoms on specific residues that were forming hydrogen bonds between the heavy and light chains of the PRX002 Fab and C-terminus of α -syn (AA 100–140), frames at which the h-bonds formed, and the donor, hydrogen, and acceptor atom ID number. The number of h-bonds per time step was calculated using the average bonds formed in each frame plotted using Matplotlib.⁵² A reverse lookup function was utilized to list the residues forming hydrogen bonds, the chains where these residues were located, and the frequency of this unique bond's appearance across all frames. To prevent percent occupancy values from exceeding 100%, a residue that forms more than one bond per frame was counted only once. PyMol was used to generate visualizations of the hydrogen bonds formed between residues.

- **2.5. RMSD Analysis.** To analyze the conformational changes in the $V_{\rm H}$ and $V_{\rm L}$ CDR regions, the root-mean-square deviation (RMSD) was calculated. VMD's RMSD analysis class was used to compute the difference between all frames of the simulation and the first frame. The PBC wrap function was used to ensure that the structure was centered in the simulation box before the RMSD calculation to prevent any periodic boundary condition-related errors. To assess how PRX002 changed over the course of each independent simulation, cluster analysis was performed with the initial frame of each system, and the final frame from each independent simulation.
- **2.6. Binding Free Energy Calculation.** To measure the binding affinity of PRX002 with α -syn, gmx_MMPBSA was used for a generalized Born (GB) and pairwise residue decomposition energy calculation. Conversions of NAMD protein structure files and trajectories to GROMACS format were performed using ParmEd and MDTraj, for respectively. The GB model was used to compute the predicted binding free energy by the following equation:

$$\Delta G_{\rm bind} = < G_{\rm com} > - < G_{\rm rec} > - < G_{\rm lig} >$$

 G_{com} , G_{rec} , and G_{lig} refer to the change in free energy of the complex, receptor, and ligand, respectively. Per-residue decomposition with 1–4 electrostatics and van der Waals added to each potential term for residues within six Angstroms between PRX002 and α -syn. All 5000 frames of each 1 μ s simulation were analyzed to determine their change in free energy.

2.7. Developability Methods. To determine the potential developability of PRX002, computational screening methods were used to determine in vitro viscosity, aggregation, and similarity to other clinical-stage therapeutics. DeepSCM was used to predict the spatial charge map (SCM) for screening potential viscosity issues. In addition, the Therapeutic Antibody Profiler (TAP)^{S7} was applied to measure total CDR length, patches of surface hydrophobicity (PSH), patches of positive charge (PPC), patches of negative charge (PNC), and the structural Fv charge symmetry parameter (SFvCSP). PSH, PPC, and PNC were all calculated metrics across the CDR vicinity. The results from TAP analysis can inform potential development issues such as aggregation and

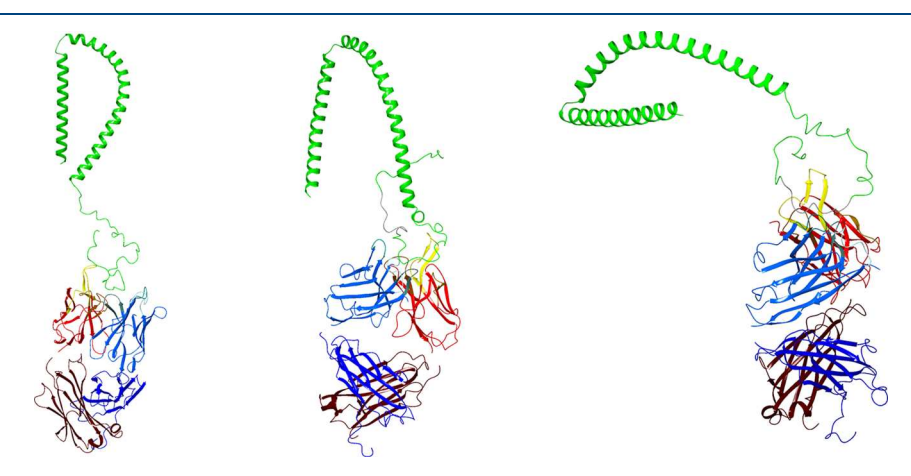


Figure 2. Complexes of the PRX002 Fab region docked with α -syn. The heavy chain of PRX002 is highlighted in blue, the light chain of PRX002 is highlighted in red, and α -syn is highlighted in green. Protein—protein docking was performed by PIPER. The C-terminus (AA 118–126, highlighted in gray) of α -syn was specified in the protein—protein docking simulation as the attraction site. (From left to right: PD-8, PD-14, and PD-27).

expression. Abpred was also used to predict the performance of the mAb on 12 biophysical platforms tested by Jain et al. 51 These experimental platforms were hydrophobic interaction chromatography (HIC), stand-up monolayer adsorption chromatography (SMAC), salt-gradient affinity-capture selfinteraction nanoparticle spectroscopy (SGAC), cross-interaction chromatography (CIC), clone self-interaction by biolayer interferometry (CSI), affinity-capture self-interaction nanoparticle spectroscopy (AC), HEK cell expression titer (HEK), polyspecificity reagent (PSR), enzyme-linked immunosorbent assay (ELISA), baculovirus particle ELISA (BVP), and differential scanning fluorimetry (DSF). These screening methods predict whether the mAb would have elevated viscosity in high concentration, its propensity for aggregation, and the similarity of the therapeutic to those of other clinicalstage mAbs.

3. RESULTS

3.1. Modeling of Antibody–Antigen Complex. Figure 2 shows the docked structures of PRX002 Fab and α -syn. PIPER docking simulations returned 10 best pose predictions, and the 3 outputs with the least distance between the CDR regions of the Fab with the C-terminus of α -syn were submitted for MD simulations. The three PRX002- α -syn complexes selected for MD simulations were 2KKW models 8, 14, and 27. (PD-8, PD-14, and PD-27). Chothia coloring schemes were utilized to highlight the specific CDR regions.

3.2. Hydrogen-Bond Analysis. Descriptive analysis of protein–protein h-bonds was performed on the outputs of each MD simulation to determine the location and frequency of intermolecular interactions over 1 μ s. Table 1a–c displays

Table 1. Most Common H-Bonds Formed^a

	(a)					
H-bond donor	H-bond acceptor	percent occupancy (%)				
Ser:H:53	Asp:A:121	55.05 ± 30.61				
Ser:H:52	Asp:A:121	41.78 ± 36.20				
Tyr:H:59	Asp:A:121	30.25 ± 42.46				
Ser:L:62	Glu:A:110	22.97 ± 31.15				
Lys:L:61	Glu:A:110	21.36 ± 29.76				
(b)						
H-bond donor	H-bond acceptor	percent occupancy (%)				
Arg:H:98	Asp:A:119	26.82 ± 37.93				
Ser:H:52	Asp:A:115	26.37 ± 37.26				
Ser:H:52	Glu:A:114	24.23 ± 28.98				
Tyr:H:59	Asp:A:115	23.99 ± 26.77				
Ser:H:53	Asp:A:115	23.03 ± 32.57				
	(c)					
H-bond donor	H-bond acceptor	percent occupancy (%)				
Lys:L:36	Asp:A:119	34.47 ± 29.27				
Ser:L:62	Glu:A:114	23.45 ± 31.25				
Lys:L:61	Glu:A:114	20.83 ± 29.45				
Tyr:H:59	Glu:A:126	19.87 ± 27.64				
Tyr:L:38	Glu:A:123	19.51 ± 27.59				

"A reverse lookup function was employed to take h-bond donor and acceptor ID numbers to list the residues on each chain forming the most h-bonds across each simulation. The top five unique residue pairs forming bonds were chosen. H = PRX002 heavy chain, L = PRX002 light chain, A = α -syn. Docked structures (a) PD8, (b) PD14, and (c) PD27.

the most prevalent bonds across the frames of the simulations. The percent occurrence of the h-bonds was calculated by averaging the bonds formed in each independent simulation and taking the standard deviation. The second heavy chain CDR (HCDR2) region of PRX002 formed the most bonds with the C-terminus of α -syn across all simulations.

3.3. Binding Affinity of Antibody—**Antigen Complex.** All 5000 frames of each of the 1 μ s simulations were analyzed for free energy estimation by gmx_MMPBSA. The resultant values for binding affinity and standard deviations were averaged across all simulations for each system. The change in binding free energy is shown in Table 2 below.

3.4. Conformational Changes in CDR Regions during Binding. Figure S1a,i displays the RMSD in Angstroms (Å) of each CDR region of PRX002 over the simulation frames. The HCDR1 region of the first and third independent simulations of PD8 has the highest average fluctuation at approximately 3 Å, which may be attributed to the amount of hydrogen bonds formed between residues on this region and α -syn. The other CDR regions across all simulations for all systems do not exceed 2.5 Å. Figure 4a-c visualizes the initial frame and final frames for each system in a cluster analysis. PRX002 is seen to move from its initial position, staying bound to the intrinsically disordered tail region of α -syn throughout the 1 μ s simulation. The second and third independent simulations of PD8 move to a similar location, while the first independent structure translates to the other side of the static representation. The same behavior is seen in PD14, as the structures rotate with α syn during the simulations. Conversely, the Fab regions of PRX002 stay in the same area in all independent simulations of PD27, with each protein's CDR regions facing the same direction.

3.5. Developability for Subcutaneous Administration. To test the developability of PRX002, DeepSCM was used to calculate the theoretical SCM score, with the mAb scoring 695.50, predicting low viscosity in high concentrations and low propensity for viscosity (the threshold value is 1000). Table 3 shows the results of the TAP analysis. TAP determined that the mAb was in range for all the measured metrics except for SFvCSP, with it scoring -6.0, just on the boundary of the amber region, predicting that the antibody design of PRX002 is comparable to those of clinical-stage therapeutics. Table 4 shows the results from Abpred, which predicted that PRX002 falls in the safe threshold for all biophysical tests, showing that the therapeutic has biophysical properties similar to those of clinical and approved mAbs.

4. DISCUSSION

Targeting aggregated α -syn has been a theorized route of treatment for years, but no medications have been developed to do so thus far. Prasinezumab is currently in Phase IIb and is the most promising candidate for an mAb targeting this pathologic protein. Understanding the mechanism by which the mAb binds to α -syn is vital for understanding its effectiveness and specific residues in the CDR regions that can be used for epitope mapping of future novel therapeutics. We simulated the three most favorable docking poses (PD8, PD14, and PD27) in triplicate for 1 μ s. Our results indicate that there exist multiple binding modes between PRX002 and α -syn. Ser:H:53-Asp:A:121 (Figure 3a) is the most prevalent hydrogen bond in PD-8. In addition, the neighbors Ser:H:52 and Asp:A:121 form the second prevalent hydrogen bond. In PD14, the top 5 hydrogen bonds show similar percent

Table 2. Binding Free Energy of PRX002 and α -syn^a

system	complex (kcal/mol)	receptor (kcal/mol)	ligand (kcal/mol)	delta (kcal/mol)
PD-8	759.3 ± 95.8	1007.14 ± 80.55	-228.72 ± 48.52	-19.11 ± 24.92
PD-14	740.78 ± 95.96	997.69 ± 80.08	-225.80 ± 47.93	-31.12 ± 30.44
PD-27	730.40 ± 100.63	975.06 ± 79.82	-219.04 ± 48.59	-25.62 ± 31.66

[&]quot;Analysis of predicted binding free energy estimates of PRX002 and α -syn simulations. All trajectories of systems PD8, PD14, and PD27 were analyzed, and values for the binding affinities were averaged.

Table 3. Therapeutic Antibody Profiler Results^a

metric	value
total CDR length	49
CDR vicinity PSH	147.4097
CDR vicinity PPC	1.1106
CDR vicinity PNC	0
SFvCSP	-6

[&]quot;Developability metrics were provided from TAP analysis. CDR = complementarity determining region, PSH = patches of surface hydrophobicity, PPC = patches of positive charge, PNC = patches of negative charge, and SFvCSP = structural Fv charge symmetry parameter.

Table 4. Abpred Biophysical Property Predictions

platform	regression	RankingRaw	ranking	nexp	threshold
HIC	9.943	68	51	134	SAFE
SMAC	-0.085	65	48	136	SAFE
SGAC	606.252	36	74	136	SAFE
CIC	0.305	85	63	136	SAFE
CSI	-0.012	58	43	136	SAFE
AC	0.581	99	73	136	SAFE
HEK	165.256	85	38	136	SAFE
PSR	0.377	117	87	136	SAFE
ELISA	2.438	111	82	136	SAFE
BVP	4.583	104	77	136	SAFE
DSF	71.285	70	49	136	SAFE
AS	0.045	49	37	136	SAFE

occupancy. Interestingly, donors Ser:H:53 and Ser:H:52 also appear in PD14, indicating the importance of these serine residues in the interaction between PRX002 and α -syn. However, the acceptors are Asp:A:115 instead of Asp:A:121 due to slightly different binding positions (Figure 4). In PD27, the hydrogen bonds form primarily between light chain PRX002 and α -syn. The most prevalent ones are Lys:L:36 and Asp:A:119 (Figure 3c). Because Lys and Asp have opposite charges, they can also form a salt bridge that further strengthens their interactions. Asp:A:119 also appears in PD14 as the most prevalent hydrogen bond (Figure 3b), showing its importance in PRX002 and α -syn interactions.

The estimated binding free energy calculated through the MM/PB(GB)SA calculation shows that PRX002 has a high affinity for α -syn. Binding affinity is a fundamental metric in drug development and discovery, and showing a strong drive for antibody—antigen binding is vital for validating Prasinezumab as a potential therapeutic. RMSD and cluster analysis show that PRX002 can flexibly move but maintains intermolecular attractions with α -syn throughout the 1 μ s simulation. The simulations were run in triplicate to both verify the occurrence of intermolecular attractions with different trajectories and to determine the ability for PRX002 to be able to maintain its bound pose with different conformations of the C-terminus of α -syn. Since we are able

to observe hydrogen bonds formed and consistent predicted binding affinity, these simulations can provide insight into the effectiveness of this mAb.

The procedures indicated in this paper provide a streamlined approach to assess the theoretical intermolecular attractions and binding affinity of a potential antibody therapeutic from sequence information alone, allowing for powerful insights early in the development process. The ability to screen mAb candidates for potential viscosity, aggregation, and other biophysical issues allows for the removal of candidates with undesirable properties, saving time and resources in the drug discovery process. Further experimental analysis to validate the intermolecular interactions between mAb and α -syn would provide more evidence to support the ongoing clinical trial of Prasinezumab.

Several different tools were used for protein—protein docking of PRX002 and α -syn. ZDock, ⁶⁰ HDock, ⁶¹ and PIPER were the rigid docking algorithm-based methods used to simulate the antibody—antigen interaction, with PIPER yielding the best results across all 34 variations of α -syn. PIPER being implemented in the BioLuminate platform also allows for easy preparation of proteins before simulation with other features as well as assigning attraction and repulsion parameters for the docking algorithm. Generating structural fingerprints from the resultant protein—protein structure is also extremely valuable for feature generation, which can be implemented in ML algorithms.

The search to cure PD has spanned decades thus far, and targeting α -syn has shown the greatest results both in the α -syn-preformed fibril model and human clinical trials. However, medications in the drug development pipeline have a high attrition rate, leading to millions of dollars put toward a medication that is either ineffective or undevelopable. Implementing computational tools such as MD for investigating the intermolecular forces, or lack thereof, will allow for quicker validation of a therapeutic agent or archiving of an ineffectual candidate.

5. CONCLUSIONS

Residues on the HCDR2 and LCDR2 of PRX002 form hbonds with the C-terminus of α -syn throughout the MD simulations performed, and PRX002 has a strong predicted affinity for α -syn. Our results show theoretically solid evidence of the binding capability of PRX002. PRX002 was also shown to not undergo drastic conformational changes after binding to α -syn and to maintain intermolecular forces with the intrinsically disordered C-terminus, showing the strong lockand-key recognition of this protein—protein complex. We propose that our method of calculating these intermolecular forces from the simulation will prove to be useful to future research of biopharmaceutical candidates for PD and beyond. In addition, we anticipate the use of this methodology in early stage development to determine the binding capabilities of biological drugs quickly.

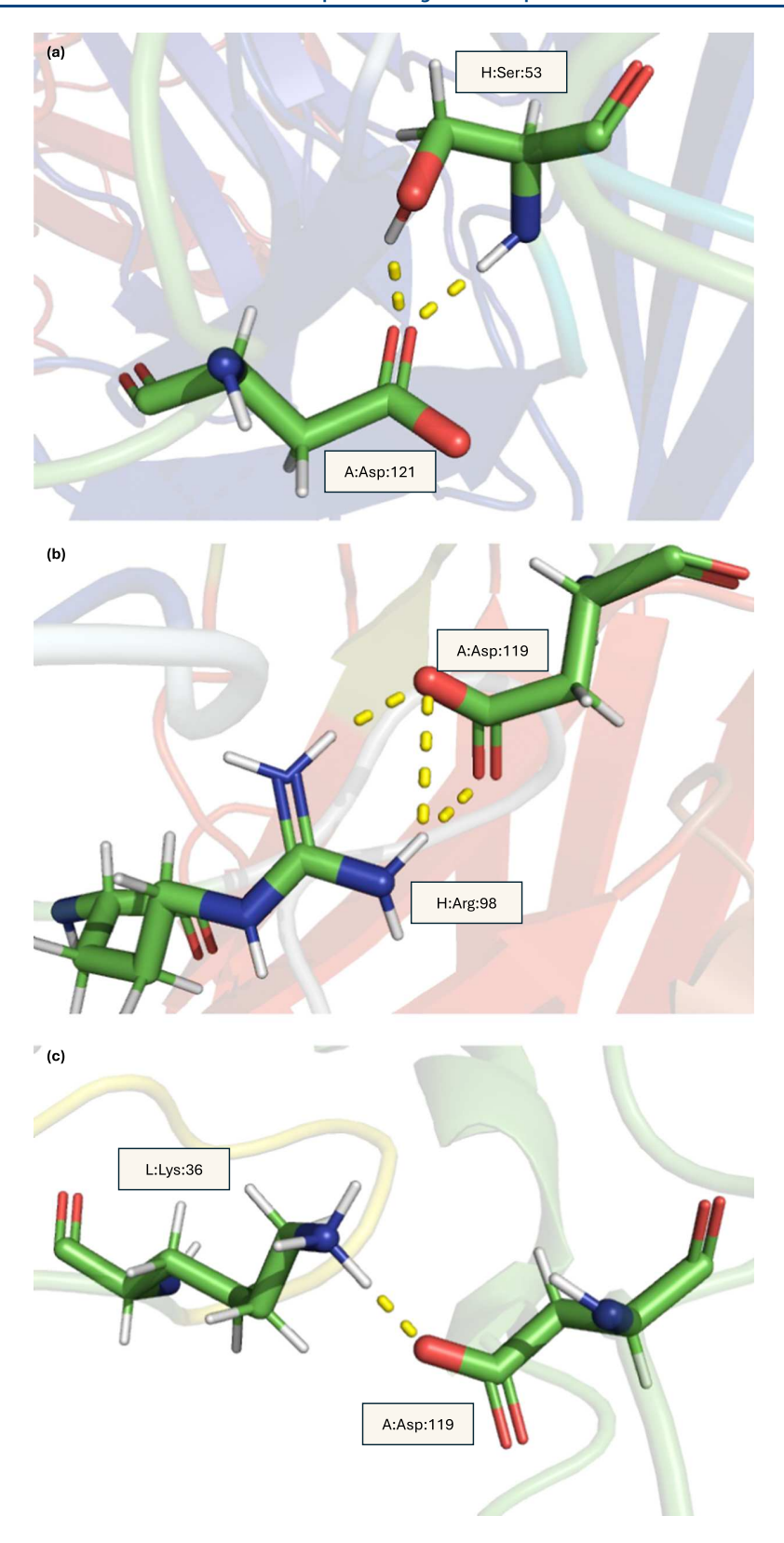
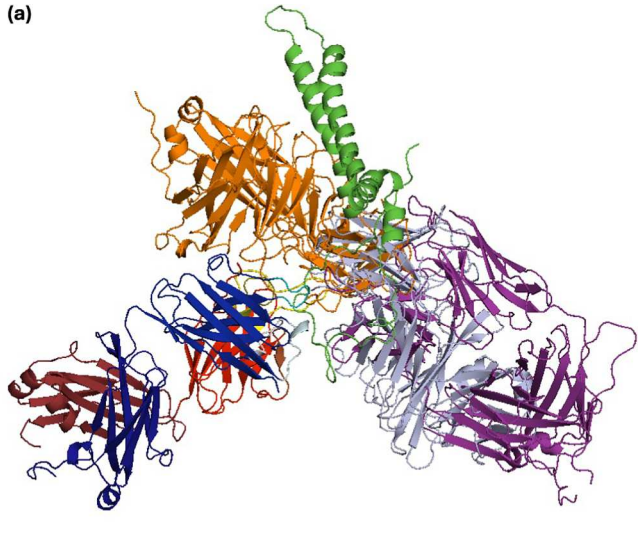
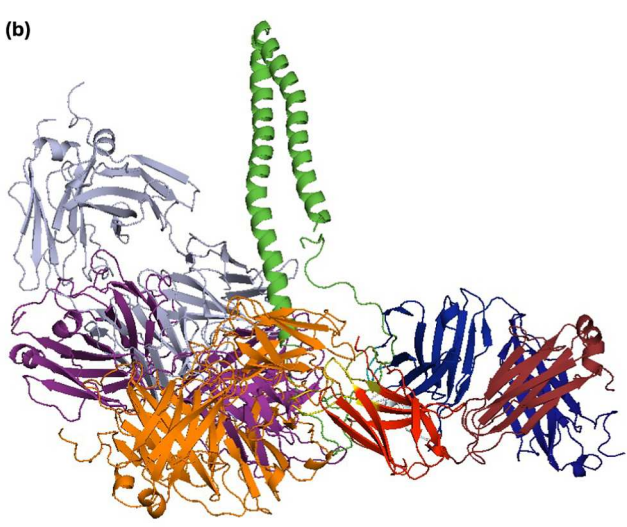


Figure 3. a—c: H-bonds formed between the variable region of PRX002, and α -syn. (a) Visualization of the h-bonds formed between serine on the PRX002 HCDR2 region and aspartic acid on α -syn for system PD8. The NH1 and OG groups on serine are the donor atoms forming the bond with an OC group on aspartic acid. The most prevalent of these two interactions is Ser:NH1-Asp:OD1. (b) Visualization of the h-bonds formed between arginine on PRX002 HCDR3 region and aspartic acid on α -syn for system PD14. Two NH2 groups on arginine are the donor atoms forming a bond with OD1 and OD2 groups on glutamic acid. The most prevalent of these two interactions is Arg:NH2-Asp:OD1. (c) Visualization of the h-bonds formed between lysine on the PRX002 LCDR1 region and aspartic acid on α -syn for PD27. The NH3 group on lysine is the donor forming the bond with the OC group on aspartic acid. H = heavy chain, L = light chain, A = α -syn, green = carbon, red = oxygen, blue = nitrogen, and white = hydrogen.





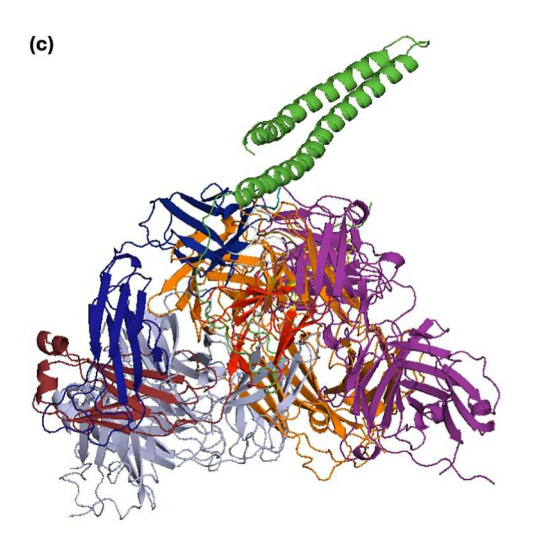


Figure 4. a—c: Cluster analysis was performed on each system with the initial frame of each system and the final frames of each independent simulation. Structures of α -syn for the final frames of each independent simulation are not shown for clarity. (a) PD8, (b) PD14, and (c) PD27. Green = α -syn, multicolor protein = initial frame of PRX002, orange = final frame of independent simulation #1, purple = final frame of independent simulation #2, and light blue = final frame of independent simulation #3.

ASSOCIATED CONTENT

Data Availability Statement

The simulation and analysis code used in this study is freely available at https://github.com/malcolmharr/Mechanistic-study-for-Parkinsons-Disease.

Supporting Information

The Supporting Information is available free of charge at https://pubs.acs.org/doi/10.1021/acs.molpharmaceut.4c00879.

Figures displaying the changes in RMSD over time during each independent simulation for PD8, PD14, and PD27 to show how the individual CDR regions of PRX002 change from their initial conformation (PDF)

AUTHOR INFORMATION

Corresponding Author

Pin-Kuang Lai — Department of Chemical Engineering and Materials Science, Stevens Institute of Technology, Hoboken, New Jersey 07030, United States; ⊚ orcid.org/0000-0003-2894-3900; Email: plai3@stevens.edu

Author

Malcolm C. Harrison – Department of Biology and Chemistry, County College of Morris, Randolph, New Jersey 07869, United States

Complete contact information is available at: https://pubs.acs.org/10.1021/acs.molpharmaceut.4c00879

Author Contributions

M.H.: conceptualization, methodology, software, data curation, formal analysis, visualization, investigation, and writing—original draft. P.-K.L.: conceptualization, methodology, software, supervision, and writing—review and editing.

Notes

The authors declare no competing financial interest.

ACKNOWLEDGMENTS

This work was supported by NSF REU/RET Site Grant #2050921. We acknowledge the computing resources provided by ACCESS (BIO220114 and CHM210013).

REFERENCES

- (1) Kouli, A.; Torsney, K. M.; Kuan, W.-L. Parkinson's Disease: Etiology, Neuropathology, and Pathogenesis. In *Parkinson's Disease: Pathogenesis and Clinical Aspects*; Stoker, T. B.; Greenland, J. C., Eds.; Codon Publications: Brisbane (AU), 2018.
- (2) Polinski, N. K.; Volpicelli-Daley, L. A.; Sortwell, C. E.; Luk, K. C.; Cremades, N.; Gottler, L. M.; Froula, J.; Duffy, M. F.; Lee, V. M. Y.; Martinez, T. N.; Dave, K. D. Best Practices for Generating and Using Alpha-Synuclein Pre-Formed Fibrils to Model Parkinson's Disease in Rodents. *J. Parkinsons Dis* **2018**, 8 (2), 303–322.
- (3) Spillantini, M. G.; Schmidt, M. L.; Lee, V. M.-Y.; Trojanowski, J. Q.; Jakes, R.; Goedert, M. α -Synuclein in Lewy Bodies. *Nature* **1997**, 388 (6645), 839–840.
- (4) Singleton, A. B.; Farrer, M.; Johnson, J.; Singleton, A.; Hague, S.; Kachergus, J.; Hulihan, M.; Peuralinna, T.; Dutra, A.; Nussbaum, R.; Lincoln, S.; Crawley, A.; Hanson, M.; Maraganore, D.; Adler, C.; Cookson, M. R.; Muenter, M.; Baptista, M.; Miller, D.; Blancato, J.; Hardy, J.; Gwinn-Hardy, K. α-Synuclein Locus Triplication Causes Parkinson's Disease. *Science* **2003**, *302* (5646), 841–841.
- (5) Ahlskog, J. E.; Muenter, M. D. Frequency of Levodopa-Related Dyskinesias and Motor Fluctuations as Estimated from the Cumulative Literature. *Movement Disorders* **2001**, *16* (3), 448–458.

- (6) Dreyer, J. K. Three Mechanisms by Which Striatal Denervation Causes Breakdown of Dopamine Signaling. *J. Neurosci.* **2014**, 34 (37), 12444–12456.
- (7) Siderowf, A.; Concha-Marambio, L.; Lafontant, D.-E.; Farris, C. M.; Ma, Y.; Urenia, P. A.; Nguyen, H.; Alcalay, R. N.; Chahine, L. M.; Foroud, T.; Galasko, D.; Kieburtz, K.; Merchant, K.; Mollenhauer, B.; Poston, K. L.; Seibyl, J.; Simuni, T.; Tanner, C. M.; Weintraub, D.; Videnovic, A.; Choi, S. H.; Kurth, R.; Caspell-Garcia, C.; Coffey, C. S.; Frasier, M.; Oliveira, L. M. A.; Hutten, S. J.; Sherer, T.; Marek, K.; Soto, C. Assessment of Heterogeneity among Participants in the Parkinson's Progression Markers Initiative Cohort Using α-Synuclein Seed Amplification: A Cross-Sectional Study. *Lancet Neurology* 2023, 22 (5), 407–417.
- (8) Wouters, O. J.; McKee, M.; Luyten, J. Estimated Research and Development Investment Needed to Bring a New Medicine to Market, 2009–2018. *JAMA* 2020, 323 (9), 844–853.
- (9) Singh, S.; Tank, N. K.; Dwiwedi, P.; Charan, J.; Kaur, R.; Sidhu, P.; Chugh, V. K. Monoclonal Antibodies: A Review. *Curr. Clin. Pharmacol.* **2018**, 13 (2), 85–99.
- (10) Lobo, E. D.; Hansen, R. J.; Balthasar, J. P. Antibody Pharmacokinetics and Pharmacodynamics. *J. Pharm. Sci.* **2004**, 93 (11), 2645–2668.
- (11) Castonguay, A.-M.; Gravel, C.; Lévesque, M. Treating Parkinson's Disease with Antibodies: Previous Studies and Future Directions. *J. Parkinsons Dis* **2021**, *11* (1), 71–92.
- (12) Castelli, M. S.; McGonigle, P.; Hornby, P. J. The Pharmacology and Therapeutic Applications of Monoclonal Antibodies. *Pharmacology Research & Perspectives* **2019**, *7* (6), No. e00535.
- (13) Lampson, L. A. Monoclonal Antibodies in Neuro-Oncology. *mAbs* **2011**, 3 (2), 153–160.
- (14) Rofo, F.; Buijs, J.; Falk, R.; Honek, K.; Lannfelt, L.; Lilja, A. M.; Metzendorf, N. G.; Gustavsson, T.; Sehlin, D.; Söderberg, L.; Hultqvist, G. Novel Multivalent Design of a Monoclonal Antibody Improves Binding Strength to Soluble Aggregates of Amyloid Beta. *Transl Neurodegener* **2021**, *10*, 38.
- (15) Sims, J. R.; Zimmer, J. A.; Evans, C. D.; Lu, M.; Ardayfio, P.; Sparks, J.; Wessels, A. M.; Shcherbinin, S.; Wang, H.; Monkul Nery, E. S.; Collins, E. C.; Solomon, P.; Salloway, S.; Apostolova, L. G.; Hansson, O.; Ritchie, C.; Brooks, D. A.; Mintun, M.; Skovronsky, D. M. TRAILBLAZER-ALZ 2 Investigators. Donanemab in Early Symptomatic Alzheimer Disease: The TRAILBLAZER-ALZ 2 Randomized Clinical Trial. *JAMA* 2023, 330 (6), 512–527.
- (16) Masliah, E.; Rockenstein, E.; Mante, M.; Crews, L.; Spencer, B.; Adame, A.; Patrick, C.; Trejo, M.; Ubhi, K.; Rohn, T. T.; Mueller-Steiner, S.; Seubert, P.; Barbour, R.; McConlogue, L.; Buttini, M.; Games, D.; Schenk, D. Passive Immunization Reduces Behavioral and Neuropathological Deficits in an Alpha-Synuclein Transgenic Model of Lewy Body Disease. *PLoS One* **2011**, *6* (4), No. e19338.
- (17) Jankovic, J.; Goodman, I.; Safirstein, B.; Marmon, T. K.; Schenk, D. B.; Koller, M.; Zago, W.; Ness, D. K.; Griffith, S. G.; Grundman, M.; Soto, J.; Ostrowitzki, S.; Boess, F. G.; Martin-Facklam, M.; Quinn, J. F.; Isaacson, S. H.; Omidvar, O.; Ellenbogen, A.; Kinney, G. G. Safety and Tolerability of Multiple Ascending Doses of PRX002/RG7935, an Anti– α -Synuclein Monoclonal Antibody, in Patients With Parkinson Disease: A Randomized Clinical Trial. *JAMA Neurology* **2018**, 75 (10), 1206–1214.
- (18) Geerts, H.; Bergeler, S.; Walker, M.; van der Graaf, P. H.; Courade, J.-P. Analysis of Clinical Failure of Anti-Tau and Anti-Synuclein Antibodies in Neurodegeneration Using a Quantitative Systems Pharmacology Model. *Sci. Rep* **2023**, *13* (1), 14342.
- (19) Pagano, G.; Taylor, K. I.; Anzures Cabrera, J.; Simuni, T.; Marek, K.; Postuma, R. B.; Pavese, N.; Stocchi, F.; Brockmann, K.; Svoboda, H.; Trundell, D.; Monnet, A.; Doody, R.; Fontoura, P.; Kerchner, G. A.; Brundin, P.; Nikolcheva, T.; Bonni, A. Prasinezumab Slows Motor Progression in Rapidly Progressing Early-Stage Parkinson's Disease. *Nat. Med.* **2024**, *30* (4), 1096–1103.
- (20) Lang, A. E.; Siderowf, A. D.; Macklin, E. A.; Poewe, W.; Brooks, D. J.; Fernandez, H. H.; Rascol, O.; Giladi, N.; Stocchi, F.; Tanner, C. M.; Postuma, R. B.; Simon, D. K.; Tolosa, E.; Mollenhauer, B.;

- Cedarbaum, J. M.; Fraser, K.; Xiao, J.; Evans, K. C.; Graham, D. L.; Sapir, I.; Inra, J.; Hutchison, R. M.; Yang, M.; Fox, T.; Budd Haeberlein, S.; Dam, T. Trial of Cinpanemab in Early Parkinson's Disease. *New England Journal of Medicine* **2022**, 387 (5), 408–420.
- (21) Sliwoski, G.; Kothiwale, S.; Meiler, J.; Lowe, E. W. Computational Methods in Drug Discovery. *Pharmacol Rev.* **2014**, 66 (1), 334–395.
- (22) Arcon, J. P.; Defelipe, L. A.; Modenutti, C. P.; López, E. D.; Alvarez-Garcia, D.; Barril, X.; Turjanski, A. G.; Martí, M. A. Molecular Dynamics in Mixed Solvents Reveals Protein—Ligand Interactions, Improves Docking, and Allows Accurate Binding Free Energy Predictions. *J. Chem. Inf. Model.* **2017**, *57* (4), 846–863.
- (23) Huang, Y.; Li, Z.; Hong, Q.; Zhou, L.; Ma, Y.; Hu, Y.; Xin, J.; Li, T.; Kong, Z.; Zheng, Q.; Chen, Y.; Zhao, Q.; Gu, Y.; Zhang, J.; Wang, Y.; Yu, H.; Li, S.; Xia, N. A Stepwise Docking Molecular Dynamics Approach for Simulating Antibody Recognition with Substantial Conformational Changes. *Computational and Structural Biotechnology Journal* **2022**, 20, 710–720.
- (24) Pawnikar, S.; Bhattarai, A.; Wang, J.; Miao, Y. Binding Analysis Using Accelerated Molecular Dynamics Simulations and Future Perspectives. Advances and Applications in Bioinformatics and Chemistry 2022, 15, 1–19.
- (25) Lai, P.-K.; Gallegos, A.; Mody, N.; Sathish, H. A.; Trout, B. L. Machine Learning Prediction of Antibody Aggregation and Viscosity for High Concentration Formulation Development of Protein Therapeutics. *mAbs* **2022**, *14* (1), No. 2026208.
- (26) Lai, P.-K. DeepSCM: An Efficient Convolutional Neural Network Surrogate Model for the Screening of Therapeutic Antibody Viscosity. Computational and Structural Biotechnology Journal 2022, 20, 2143–2152.
- (27) Yu, H.; Han, W.; Ma, W.; Schulten, K. Transient β -Hairpin Formation in α -Synuclein Monomer Revealed by Coarse-Grained Molecular Dynamics Simulation. *J. Chem. Phys.* **2015**, *143* (24), 243142.
- (28) Tripathi, P.; Ganeshpurkar, A.; Singh, S. K.; Krishnamurthy, S. Identification of Novel Glucocerebrosidase Chaperone for Potential Treatment of Parkinson's Disease: An Approach Using *in Silico* Virtual Screening, Molecular Docking and Molecular Dynamics, and in Vitro Studies. *Int. J. Biol. Macromol.* 2023, 228, 453–466.
- (29) Robustelli, P.; Ibanez-de-Opakua, A.; Campbell-Bezat, C.; Giordanetto, F.; Becker, S.; Zweckstetter, M.; Pan, A. C.; Shaw, D. E. Molecular Basis of Small-Molecule Binding to α -Synuclein. *J. Am. Chem. Soc.* **2022**, 144 (6), 2501–2510.
- (30) Iqbal, D.; Rehman, M. T.; Bin Dukhyil, A.; Rizvi, S. M. D.; Al Ajmi, M. F.; Alshehri, B. M.; Banawas, S.; Khan, M. S.; Alturaiki, W.; Alsaweed, M. High-Throughput Screening and Molecular Dynamics Simulation of Natural Product-like Compounds against Alzheimer's Disease through Multitarget Approach. *Pharmaceuticals* **2021**, *14* (9), 937.
- (31) Heikkilä, V.-M.; Turkka, J.; Korpelainen, J.; Kallanranta, T.; Summala, H. Decreased Driving Ability in People with Parkinson's Disease. *Journal of Neurology, Neurosurgery & Psychiatry* **1998**, *64* (3), 325–330.
- (32) Li, L.; Kumar, S.; Buck, P. M.; Burns, C.; Lavoie, J.; Singh, S. K.; Warne, N. W.; Nichols, P.; Luksha, N.; Boardman, D. Concentration Dependent Viscosity of Monoclonal Antibody Solutions: Explaining Experimental Behavior in Terms of Molecular Properties. *Pharm. Res.* **2014**, *31* (11), 3161–3178.
- (33) KEGG DRUG: Prasinezumab. https://www.genome.jp/entry/D11420 (accessed 2024-02-19).
- (34) Sankar, K.; Trainor, K.; Blazer, L. L.; Adams, J. J.; Sidhu, S. S.; Day, T.; Meiering, E.; Maier, J. K. X. A Descriptor Set for Quantitative Structure-Property Relationship Prediction in Biologics. *Molecular Informatics* **2022**, 41 (9), No. 2100240.
- (35) Tavella, D.; Ouellette, D. R.; Garofalo, R.; Zhu, K.; Xu, J.; Oloo, E. O.; Negron, C.; Ihnat, P. M. A Novel Method for in Silico Assessment of Methionine Oxidation Risk in Monoclonal Antibodies: Improvement over the 2-Shell Model. *PLoS One* **2022**, *17* (12), No. e0279689.

- (36) Sankar, K.; Krystek, S. R.; Carl, S. M.; Day, T.; Maier, J. K. X. AggScore: Prediction of Aggregation-Prone Regions in Proteins Based on the Distribution of Surface Patches. *Proteins* **2018**, *86* (11), 1147–1156.
- (37) Salam, N. K.; Adzhigirey, M.; Sherman, W.; Pearlman, D. A. Structure-Based Approach to the Prediction of Disulfide Bonds in Proteins. *Protein Engineering, Design and Selection* **2014**, 27 (10), 365–374.
- (38) Beard, H.; Cholleti, A.; Pearlman, D.; Sherman, W.; Loving, K. A. Applying Physics-Based Scoring to Calculate Free Energies of Binding for Single Amino Acid Mutations in Protein-Protein Complexes. *PLoS One* **2013**, *8* (12), No. e82849.
- (39) Schrödinger, LLC. The PyMOL Molecular Graphics System, Version 1.8, 2015.
- (40) Bank R. P. D. RCSB PDB 2KKW: SLAS-micelle bound alphasynuclein. https://www.rcsb.org/structure/2KKW (accessed 2024-08-05).
- (41) Madhavi Sastry, G.; Adzhigirey, M.; Day, T.; Annabhimoju, R.; Sherman, W. Protein and Ligand Preparation: Parameters, Protocols, and Influence on Virtual Screening Enrichments. *J. Comput. Aided Mol. Des* **2013**, 27 (3), 221–234.
- (42) Chuang, G.-Y.; Kozakov, D.; Brenke, R.; Comeau, S. R.; Vajda, S. DARS (Decoys As the Reference State) Potentials for Protein-Protein Docking. *Biophys. J.* **2008**, 95 (9), 4217–4227.
- (43) Kozakov, D.; Brenke, R.; Comeau, S. R.; Vajda, S. PIPER: An FFT-Based Protein Docking Program with Pairwise Potentials. *Proteins* **2006**, *65* (2), 392–406.
- (44) Humphrey, W.; Dalke, A.; Schulten, K. VMD: Visual Molecular Dynamics. *J. Mol. Graphics* **1996**, *14* (1), 33–38.
- (45) Phillips, J. C.; Hardy, D. J.; Maia, J. D. C.; Stone, J. E.; Ribeiro, J. V.; Bernardi, R. C.; Buch, R.; Fiorin, G.; Hénin, J.; Jiang, W.; McGreevy, R.; Melo, M. C. R.; Radak, B. K.; Skeel, R. D.; Singharoy, A.; Wang, Y.; Roux, B.; Aksimentiev, A.; Luthey-Schulten, Z.; Kalé, L. V.; Schulten, K.; Chipot, C.; Tajkhorshid, E. Scalable Molecular Dynamics on CPU and GPU Architectures with NAMD. *J. Chem. Phys.* 2020, 153 (4), No. 044130.
- (46) Huang, J.; Rauscher, S.; Nawrocki, G.; Ran, T.; Feig, M.; de Groot, B. L.; Grubmüller, H.; MacKerell, A. D. CHARMM36m: An Improved Force Field for Folded and Intrinsically Disordered Proteins. *Nat. Methods* **2017**, *14* (1), 71–73.
- (47) MacKerell, A. D., Jr.; Bashford, D.; Bellott, M.; Dunbrack, R. L., Jr.; Evanseck, J. D.; Field, M. J.; Fischer, S.; Gao, J.; Guo, H.; Ha, S.; Joseph-McCarthy, D.; Kuchnir, L.; Kuczera, K.; Lau, F. T. K.; Mattos, C.; Michnick, S.; Ngo, T.; Nguyen, D. T.; Prodhom, B.; Reiher, W. E.; Roux, B.; Schlenkrich, M.; Smith, J. C.; Stote, R.; Straub, J.; Watanabe, M.; Wiórkiewicz-Kuczera, J.; Yin, D.; Karplus, M. All-Atom Empirical Potential for Molecular Modeling and Dynamics Studies of Proteins. *J. Phys. Chem. B* 1998, 102 (18), 3586–3616.
- (48) Darden, T.; York, D.; Pedersen, L. Particle Mesh Ewald: An Nlog(N) Method for Ewald Sums in Large Systems. *J. Chem. Phys.* 1993, 98 (12), 10089–10092.
- (49) Gowers, R. J.; Linke, M.; Barnoud, J.; Reddy, T. J. E.; Melo, M. N.; Seyler, S. L.; Domański, J.; Dotson, D. L.; Buchoux, S.; Kenney, I. M.; Beckstein, O. MDAnalysis: A Python Package for the Rapid Analysis of Molecular Dynamics Simulations. In *Proceedings of the 15th Python in Science Conference*; Benthall, S.; Rostrup, S., Eds.; LANL: 2016; pp. 98–105.
- (50) Michaud-Agrawal, N.; Denning, E. J.; Woolf, T. B.; Beckstein, O. MDAnalysis: A Toolkit for the Analysis of Molecular Dynamics Simulations. *J. Comput. Chem.* **2011**, 32 (10), 2319–2327.
- (51) Harris, C. R.; Millman, K. J.; van der Walt, S. J.; Gommers, R.; Virtanen, P.; Cournapeau, D.; Wieser, E.; Taylor, J.; Berg, S.; Smith, N. J.; Kern, R.; Picus, M.; Hoyer, S.; van Kerkwijk, M. H.; Brett, M.; Haldane, A.; del Río, J. F.; Wiebe, M.; Peterson, P.; Gérard-Marchant, P.; Sheppard, K.; Reddy, T.; Weckesser, W.; Abbasi, H.; Gohlke, C.; Oliphant, T. E. Array Programming with NumPy. *Nature* **2020**, 585 (7825), 357–362.
- (52) Hunter, J. D. Matplotlib: A 2D Graphics Environment. Computing in Science & Engineering 2007, 9 (3), 90–95.

- (53) Valdés-Tresanco, M. S.; Valdés-Tresanco, M. E.; Valiente, P. A.; Moreno, E. gmx_MMPBSA: A New Tool to Perform End-State Free Energy Calculations with GROMACS. *J. Chem. Theory Comput.* **2021**, *17* (10), 6281–6291.
- (54) Abraham, M. J.; Murtola, T.; Schulz, R.; Páll, S.; Smith, J. C.; Hess, B.; Lindahl, E. GROMACS: High Performance Molecular Simulations through Multi-Level Parallelism from Laptops to Supercomputers. *SoftwareX* **2015**, *1*–2, 19–25.
- (55) Shirts, M. R.; Klein, C.; Swails, J. M.; Yin, J.; Gilson, M. K.; Mobley, D. L.; Case, D. A.; Zhong, E. D. Lessons Learned from Comparing Molecular Dynamics Engines on the SAMPLS Dataset. *J. Comput. Aided Mol. Des* **2017**, *31* (1), 147–161.
- (56) McGibbon, R. T.; Beauchamp, K. A.; Harrigan, M. P.; Klein, C.; Swails, J. M.; Hernández, C. X.; Schwantes, C. R.; Wang, L.-P.; Lane, T. J.; Pande, V. S. MDTraj: A Modern Open Library for the Analysis of Molecular Dynamics Trajectories. *Biophys. J.* **2015**, *109* (8), 1528–1532.
- (57) Raybould, M. I. J.; Marks, C.; Krawczyk, K.; Taddese, B.; Nowak, J.; Lewis, A. P.; Bujotzek, A.; Shi, J.; Deane, C. M. Five Computational Developability Guidelines for Therapeutic Antibody Profiling. *Proc. Natl. Acad. Sci. U. S. A.* **2019**, *116* (10), 4025–4030.
- (58) Hebditch, M.; Warwicker, J. Charge and Hydrophobicity Are Key Features in Sequence-Trained Machine Learning Models for Predicting the Biophysical Properties of Clinical-Stage Antibodies. *PeerJ.* **2019**, *7*, No. e8199.
- (59) Jain, T.; Sun, T.; Durand, S.; Hall, A.; Houston, N. R.; Nett, J. H.; Sharkey, B.; Bobrowicz, B.; Caffry, I.; Yu, Y.; Cao, Y.; Lynaugh, H.; Brown, M.; Baruah, H.; Gray, L. T.; Krauland, E. M.; Xu, Y.; Vásquez, M.; Wittrup, K. D. Biophysical Properties of the Clinical-Stage Antibody Landscape. *Proc. Natl. Acad. Sci. U. S. A.* **2017**, *114* (5), 944–949.
- (60) Pierce, B. G.; Wiehe, K.; Hwang, H.; Kim, B.-H.; Vreven, T.; Weng, Z. ZDOCK Server: Interactive Docking Prediction of Protein—Protein Complexes and Symmetric Multimers. *Bioinformatics* **2014**, 30 (12), 1771–1773.
- (61) Yan, Y.; Tao, H.; He, J.; Huang, S.-Y. The HDOCK Server for Integrated Protein—Protein Docking. *Nat. Protoc* **2020**, *15* (5), 1829—1852.